PHYSICAL REVIEW B **93**, 121302(R) (2016)

Two-dimensional optical nanovortices at visible light

Asaf David, Bergin Gjonaj, and Guy Bartal
Department of Electrical Engineering, Technion–Israel Institute of Technology, Technion City 3200000, Haifa, Israel
(Received 10 December 2015; revised manuscript received 16 February 2016; published 9 March 2016)

Optical vortices possess unique topology which can benefit a broad variety of applications, ranging from particle trapping and microscopy to communications and light-matter interactions. Notwithstanding their proven applicability, being subjected to the diffraction limit typically inhibits the facilitation of vortex beams into nanoscale applications. Here, we present optical nanovortices of 60 nm size employing silicon-based waveguides that support guided modes with short wavelengths. We introduce nanovortices with on-demand topological charge and show azimuthal phase variations almost ten times faster than free-space oscillations of the illumination wavelength (671 nm) using high-resolution phase-resolved near-field measurements. Moreover, we apply superoscillations of two short-wavelength guided modes to further decrease the radial size of the vortex, achieving nanosized dimensions in both the azimuthal and radial directions.

DOI: 10.1103/PhysRevB.93.121302

Optical vortices (OVs) are unique physical phenomena where the phase of light rotates around a central singular point, creating a dark spot surrounded by a ring of bright light. OVs carry an orbital angular momentum (OAM) that can be converted into a mechanical torque [1], making them attractive candidates for potential applications such as small-scale optical communications between chips [2], high capacity wireless communications [3], optical trapping [4–7], particle spinning [8], and micromechanical optically induced rotations [9]. The singular nature of the zero-amplitude point is well exploited in super-resolution microscopy [10]. In a broader context, vortices have been demonstrated and are being used in, e.g., x-ray [11], millimeter [3], and acoustic waves [12] as well as nonlinear optics [13,14].

The size of the optical vortex determines the smallest length scale of interaction and therefore governs the ability of applications to rotate nanoparticles, miniaturize optical communication devices, and further enhance super-resolution capabilities. Moreover, it can open new opportunities in light-matter interactions via OAM exchange. However, the diffractive nature of light waves imposes limitations on the smallest size of the vortex, hence limiting the interaction with quantum emitters placed in the vicinity of the singularity due to a large zero-amplitude area. Recent works [15,16] have shown that chiral structures with modes resembling subwavelengh optical vortices allow for directional emission of quantum dots and are in the front line of quantum optics research. Reducing the size of OVs to the scale of quantum systems (tens of nm for quantum dots) has the potential to provide new directions in both fundamental and applied science.

Here, we present direct observation of optical nanovortices utilizing short-wavelength hybrid photonic-plasmonic (HPP) modes. We show phase-resolved optical vortices in two dimensions carrying a well determined topological charge with feature sizes as small as tens of nanometers at 671 nm illumination. We demonstrate a direct near-field mapping of azimuthal 2π phase rotation along a 75 nm circumference at this wavelength and further engineer dual-mode waveguides so as to create superoscillations of two individual vortices to achieve OVs approaching the size of a single quantum dot. In doing so, we achieve and directly measure an optical vortex whose phase oscillates faster than its wavelength in both the radial and the azimuthal directions, namely, *radial-azimuthal superoscillations*.

Two-dimensional (2D) OVs can be created either on the focal plane of helical beams, or by propagating surface modes on a two-dimensional plane [17–19]. The first type is usually described as Laguerre-Gaussian (LG) beams [1], which typically propagates normal to the vortex plane. Conversely, the surface modes are two-dimensional vortices which exponentially decay in the direction normal to the interface. Being two dimensional, the mathematical description of the surface optical vortex is that of the cylindrical harmonics with the radial part given by Bessel functions of the first kind,

$$E_{z,l}(\rho,\phi,z) = E_0 J_l(k_r\rho)\exp(il\phi)\exp(-k_z z), \qquad (1)$$

where J_l is the lth-order Bessel function of the first kind, ρ, ϕ, and z are the cylindrical coordinate set, and k_r and k_z are the wave numbers in and normal to the surface, respectively. The order l of the Bessel function is always similar to the number of periods the phase completes in the azimuthal direction within a full circle and is referred to as the topological charge of the vortex. Two-dimensional optical vortices have been demonstrated in plasmonic structures [17,19], though until recently [20] they were always subjected to a diffraction-limited size and thus have not been significantly downscaled relative to the free-space wavelength.

We create optical vortices that are downscaled in size (nanovortices) by coupling circularly polarized light into short-wavelength guided modes by means of an optical spin-orbit interaction [17,18]. Figure 1(a) presents a conceptual description of optical vortices generated on a planar Si-based waveguide. The waveguide is a layered structure consisting of a thin Si layer atop a metallic substrate (silver or gold) separated by nanometers-thick silicon dioxide (SiO_2), which supports a hybridization of photonic modes and surface-plasmon polaritons [20,22]. The high index of the guided modes results in short wavelengths which downscale the size of the vortices. Circularly polarized light of 671 nm wavelength is coupled into the guided mode by thin slits milled by a focused ion beam (FIB). The coupling slits milled into the platform are designed as spiral-shaped two-dimensional lenses so as to focus the hybrid modes into a vortex beam by providing the appropriate geometrical phase: While the circularly polarized

light provides an OAM of ± 1 (depending on the direction of rotation), the 2D lens adds an integer number that is equal to the geometric topological charge of the lens. The sum of the light's OAM and the lens' geometrical topological charge equals the topological charge of the vortex [17,19]. To directly observe the topological charge of the nanovortices we use a scattering type near-field scanning optical microscope (s-NSOM) [Neaspec Ltd., experimental setup is described in Fig. 1(b)] that enables phase-resolved mapping of the near field on the surface from the Si side [21]. The Atomic Force Microscope (AFM) tip is metal coated ($PtIr_5$ coating, Nano World Ltd.) and mainly scatters the out-of-plane component of the near field. The 3D visualizations of the measured phase pattern in the focus of such a structure, shown in Fig. 1(a), demonstrate topological charges of $l = 3$ and $l = 5$ obtained by coupling left-handed and right-handed circularly polarized light by a lens with a topological charge of 4.

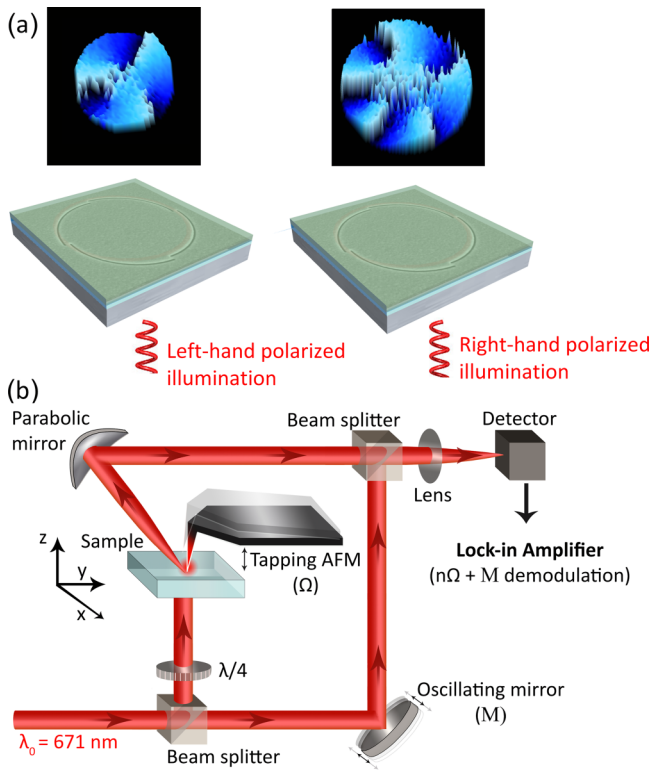

FIG. 1. (a) Near-field imaging of two-dimensional nanovortices. Circularly polarized light (671 nm) is coupled into a silicon waveguide via a spiral-shaped slit. A scanning electron microscope (SEM) image shows the slit design as a broken Archimedean spiral with a topological charge of 4, milled from the silver side of the platform. The near-field measured phase pattern is a vortex pattern of order 3 for left-handed polarization or 5 for right-handed polarization. (b) Transmission mode near-field microscopy setup. The sample is illuminated from underneath by a weakly focused 671 nm laser beam. The evanescent tail of the coupled guided modes is scattered by an atomic force microscope tip and directed towards a detector where it interferes with a reference beam. The tip oscillates at a frequency $\Omega = 250$ kHz while a piezoelectric driven mirror oscillates the phase of the reference beam at a frequency $M = 600$ Hz. The direct far-field background is filtered by demodulating the signal on the detector at higher harmonics $n\Omega$ [21]. The near-field amplitude and phase maps are acquired by scanning the sample.

We begin by presenting a direct measurement of the topological charge of optical nanovortices in a single-mode short-wavelength waveguide. Figure 2 shows phase-resolved near-field measurements of scaled 2D optical vortices with topological charges of $l = 1, 2$, and 5 using spiral lenses of the order $m = 0$ (circular lens), $m = 1$, and $m = 4$, respectively. The waveguide used for this demonstration is a Si-SiO_2-Ag waveguide with layer thicknesses of 60 nm–7 nm–250 nm, respectively. This configuration supports a single guided mode with an effective index of $n_{\text{eff}} = 3.05$, resulting in a mode wavelength of $\lambda_m = 2\pi/k_m = 220$ nm [20]. The generated phase patterns clearly demonstrate the topological charge of the vortices, which is equal to the number of 2π phase periods in the inner circle. The size of the vortices is downscaled according to the mode index: The position of the first intensity peak equals $r_{\text{peak}} = p_l \lambda_0 / 2\pi n_{\text{eff}}$ (where p_l is the first peak in the lth-order Bessel function). The first intensity ring is therefore of $r_{\text{peak}} = 70 \pm 5$ nm radius (for $l = 1$), creating a dark

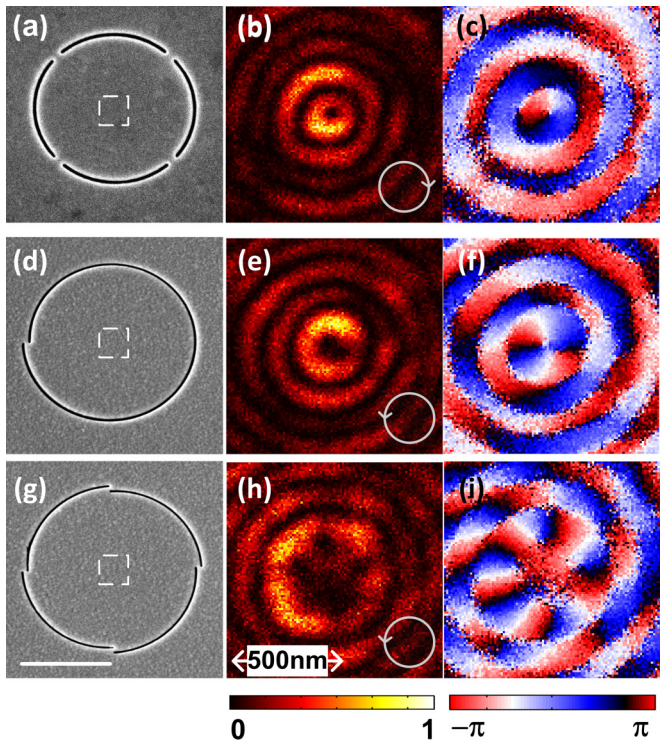

FIG. 2. Observation of topological charge of nanovortices in a 2D Si waveguide. Phase-resolved near-field measurements of a single guided short-wavelength mode (mode wavelength $\lambda_m = 220$ nm at an illumination wavelength of $\lambda_0 = 671$ nm) focused into optical vortices via 2D lenses illuminated with circularly polarized light. (a) SEM image of a circular 2D lens (geometrical topological charge 0) creating an optical vortex with a topological charge $l = 1$ (bright spot) for right-handed circular polarized light, as shown in the near-field maps of the measured intensity (b) and phase (c). (d)–(f) Similarly, right-handed circular polarization creates a vortex with a topological charge $l = 2$ when an Archimedian spiral-shaped lens (geometric topological charge 1) is used. (g)–(j) An Archimedian spiral lens with geometrical topological charge 4 focuses the guided modes into a nanovortex with a topological charge of $l = 5$. The length of the scale bar in the SEM images is 3 μm. The location of the scanned areas corresponds to the dashed squares in the SEM images.

spot with a full width at half maximum (FWHM) of 80 ± 5 nm. Previous works, for comparison, reported on an observation of a first intensity ring with a radius of 180 nm with a similar excitation wavelength [19]. The radius of the inner phase circle (in which the phase flips sign for the first time) is $r_{\text{phase}} = 125 \pm 10$ nm [Fig. 2(c)]. Likewise, the $l = 2$ ring depicts an intensity ring of $r_{\text{peak}} = 110 \pm 5$ nm radius and $r_{\text{phase}} = 180 \pm 10$ nm radius phase flip, while the $l = 5$ ring displays radii of $r_{\text{peak}} = 230 \pm 10$ nm and $r_{\text{phase}} = 310 \pm 10$ nm, respectively.

Interestingly, the azimuthal phase variation does not depend on the radius and hence can become arbitrarily fast close to the singularity point. In particular, at radii deciding $r < \lambda_m l/2\pi$, where l is the optical charge of the vortex, the oscillations become faster than the system's diffraction limit. While its similarity to superoscillatory behavior was indicated by Berry [23], these fast oscillations have not been so far directly observed, owing to the attenuation of the amplitude accompanying such oscillations at these radii, as well as the difficulties in measuring phase oscillations at such a super-resolution. Our ability to downscale the vortex on one hand, and measure the phase of the near field in a resolution below 15 nm on the other, enables us to map these fast phase oscillations and demonstrate such azimuthal "super-oscillations," even with respect to the downscaled wavelength. Figure 3 shows direct experimental demonstration of such fast oscillations by mapping the azimuthal phase accumulation over the circumference of a circle at small radii in two of the vortices presented in Fig. 2. Figure 3(a) draws the phase around a circle at an average distance of $r_1 = 12$ nm from the center of the optical vortex with a topological charge of $l = 1$. We show a full 2π phase accumulation along a circumference of 75 nm, which is three times smaller than λ_m and nine times smaller than λ_0. Figure 3(b) depicts a similar procedure for an optical vortex with a topological charge $l = 2$ at an averaged radius of $r_2 = 42$ nm, showing a 4π accumulation over a circumference of 264 nm, corresponding to a full cycle of 132 nm at the same excitation wavelength. Although in principle such a measurement could have been demonstrated on larger optical vortices, the energy density relative to the total power at this small radius is larger compared to a larger-scale vortex, which assists the measurement by providing a better signal-to-noise ratio (SNR).

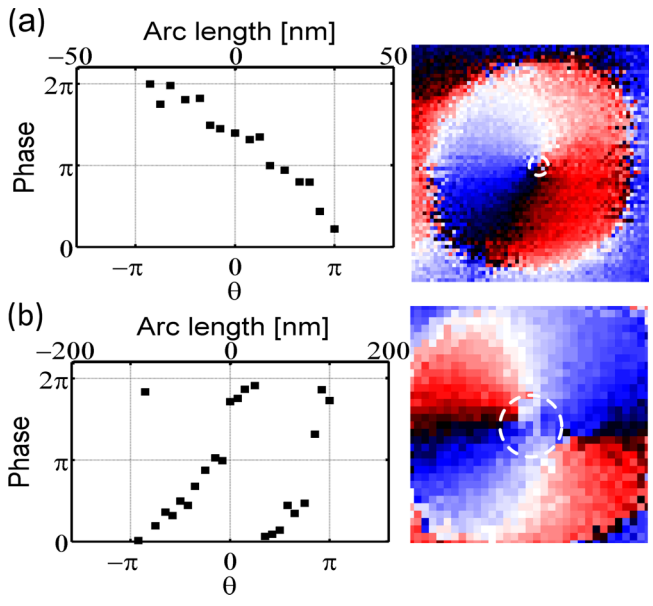

FIG. 3. Azimuthal superoscillations. (a) Azimuthal phase accumulation in a vortex beam with a topological charge of 1 at a small radius ($r_1 = 12 \pm 2$ nm), showing a 2π phase accumulation over 75 nm. (b) Azimuthal phase accumulation in a vortex beam with a topological charge of 2 at a small radius ($r_2 = 42 \pm 2$ nm), showing a 4π accumulation over 264 nm. The closeup phase measurement images (320 nm × 320 nm) on the right-hand side show in the white circle the data points that are presented in the phase plots.

While azimuthal "superoscillations" occur naturally around the vortex's singularity, a careful design of multiple short-wavelength modes can lead to superoscillatory behavior in the radial direction as well. Radial superoscillations (RSOs) emerge when two or more coherent modes interfere [24,25], with the beating pattern containing oscillations faster than the wavelength. Increasing the Si layer thickness in the HPP waveguide to above 100 nm leads to a dual-mode operation, where each of the modes can be engineered independently by changing the layer thicknesses (see Ref. [20]). When circularly polarized light is coupled into such a waveguide through a two-dimensional lens, an interference pattern of two equally centered optical vortices is generated according to Eq. (1). The beating pattern is described as

$$\begin{aligned} E_{z,\text{int}}(\rho,\phi,z) = {} & a_1 J_l(k_{r,1}\rho)\exp(il\phi)\exp(-k_{z,1}z) \\ & + a_2 J_m(k_{r,2}\rho)\exp(im\phi)\exp(-k_{z,2}z) \\ & \times \exp(i\Delta\varphi), \end{aligned} \tag{2}$$

where a_1 and a_2 are the amplitudes of the two vortices and $\Delta\varphi$ is the phase difference between the fields in the center of the vortices. Figure 4 shows the beating pattern of two optical vortices associated with the two guided modes in a Si-SiO_2-Au waveguide with layer thicknesses of 160 nm–22 nm–170 nm, respectively. For a free-space wavelength of $\lambda_0 = 671$ nm, the mode indices of the guided modes are $n_{\text{eff},1} = 3.35$ and $n_{\text{eff},2} = 2.38$, creating mode wavelengths of $\lambda_{m,1} = 200$ nm and $\lambda_{m,2} = 282$ nm, respectively. Illuminating circularly polarized light on a circular slit, which is wavelength independent, we obtain a beating pattern between two concentric optical vortices with a topological charge of $l = 1$ corresponding to each of the guided modes.

While superoscillation features are generally low in intensity, a proper design of the coupling can position the RSO about the center of the vortex, where the intensity is enhanced by the focusing. As local superoscillations occur on the beating minima, where the relative phase between the two modes is π, the radius of the circular coupling slit R should conform to the phase condition

$$\Delta\varphi = \arg[H_1(k_1 R)] - \arg[H_1(k_2 R)] = N\pi, \tag{3}$$

where $H_1(x)$ is the first-order Hankel's function of the first kind, which is the propagator of the field on a flat surface, and N is an integer number. When $k_i R \gg 1/4$, we can use Hankel's function approximation to achieve the phase condition in Eq. (3) by choosing $R \simeq (N + 1/2)\lambda_{\text{beat}}$, where $\lambda_{\text{beat}} = \lambda_{m,1}\lambda_{m,2}/(\lambda_{m,1} - \lambda_{m,2})$ is the period of beating between the

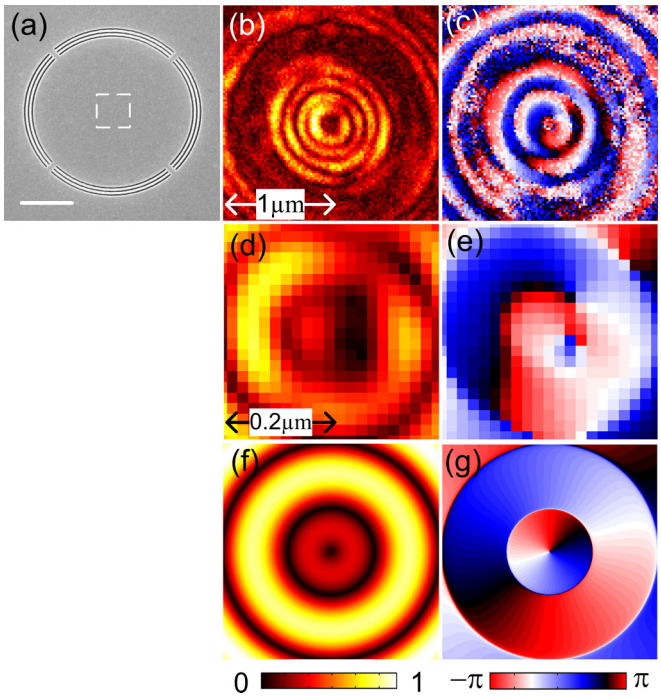

FIG. 4. Radial-azimuthal superoscillations. Near-field measurements for circularly polarized light coupled by a $r = 4.51\ \mu$m circular slit milled into a dual-mode Si-SiO_2-Au waveguide. The layer thicknesses are 160 nm–22 nm–170 nm, and the mode wavelengths are $\lambda_{m,1} = 200 \pm 5$ nm and $\lambda_{m,2} = 282 \pm 5$ nm. (a) SEM image of the coupling slit. The slit consists of a grating with 195 nm periodicity for introducing more energy into the system and improving the coupling efficiency of the short-wavelength mode. (b)–(e) Beating pattern and superoscillations of two modes with short wavelength. The 2 μm × 2 μm near-field amplitude (b) and phase (c) mapping show the beating pattern of the two modes. The superoscillations appear in 400 nm × 400 nm closeup images of the amplitude (d) and phase (e) of the measurements after filtering in the Fourier domain to remove the background. (f), (g) Simulation of the beating pattern show the amplitude (f) and phase (g) of superoscillations showing phase characteristics that are similar to the measured ones.

modes. Similarly, the amplitude condition $a_1 \sim a_2$ should be met at the superoscillation location in order to maximize the contrast. We achieve this condition by balancing the different propagation lengths of the modes that are preferential to mode 1 ($L_1 = 5.4\ \mu$m and $L_2 = 2.2\ \mu$m, according to numerical calculations) with the different coupling efficiencies that are preferential to mode 2. Choosing $R = 4.51\ \mu$m ($N = 5$) accurately balances the different coupling coefficients with the difference in the propagation length, resulting in visible RSOs [Figs. 4(d) and 4(e)]. The combination of the radial superoscillations achieved by the two mode interferences and the azimuthal ones created by the optical vortex results in a phase pattern with a central phase ring whose radius equals $r_{\text{phase}} = 60 \pm 5$ nm, which is half the size of the single-mode vortex shown in Fig. 2, corresponding to a local wavelength of 120 nm (or an intensity ring radius $r_{\text{peak}} = 30$ nm), which also rotates azimuthally arbitrarily fast. The measured [Figs. 4(c) and 4(e)] and simulated [Fig. 4(g)] phase patterns clearly show the radial-azimuthal superoscillation effect of azimuthal superoscillation located in a circle that is much smaller than the (already downscaled) diffraction limit.

We have shown phase-resolved near-field measurements of two-dimensional optical vortices with various topological charges on a silicon-based waveguide supporting hybrid photonic-plasmonic guided modes. The optical vortices are downscaled in size due to the high mode index, resulting in sub-100-nm dark spots. Furthermore, we demonstrate direct observation of an azimuthal superoscillating phase in single-mode vortices and radial-azimuthal superoscillations in dual-mode vortices. Our observations are an experimental demonstration of superoscillations in vortices in the optical regime. Reducing the size of the optical vortices has potential applications for super-resolution microscopy, optical tweezers for small-scale particles, and nanoscale optical spinning. In addition, downscaled optical vortices bring the size of the light carrying the orbital momentum closer to the size of quantum systems while carrying sufficient energy to allow for different investigations of OAM-based interactions of light with quantum systems.

For helpful discussions and graphical assistance we acknowledge Meir Orenstein and Anouk de-Hooch. The fabrication in this work was supported by the Russell Berrie Nanotechnology Institute (RBNI) and the Micro Nano Fabrication Unit (MNFU) at the Technion. We acknowledge support from the ICORE Excellence Center "Circle of Light"; B. G. acknowledges that: The research leading to these results has received funding from the European Union's - Seventh Framework Programme (FP7/2007-2013]) under Grant Agreement No. 626812 MC–MultiSPLASH.

[1] L. Allen, M. W. Beijersbergen, R. J. C. Spreeuw, and J. P. Woerdman, Phys. Rev. A **45**, 8185 (1992).
[2] X. Cai, J. Wang, M. Strain, B. Johnson-Morris, J. Zhu, M. Sorel, J. O'Brien, M. Thompson, and S. Yu, Science **338**, 363 (2012).
[3] Y. Yan, G. Xie, M. P. J. Lavery, H. Huang, N. Ahmed, C. Bao, Y. Ren, Y. Cao, L. Li, Z. Zhao, A. F. Molisch, M. Tur, M. J. Padgett, and A. E. Willner, Nat. Commun. **5**, 4876 (2014).
[4] K. T. Gahagan and G. A. Swartzlander, Jr., Opt. Lett. **21**, 827 (1996).
[5] D. G. Grier, Nature (London) **424**, 810 (2003).
[6] K. Ladavac and D. G. Grier, Opt. Express **12**, 1144 (2004).
[7] J. E. Curtis and D. G. Grier, Phys. Rev. Lett. **90**, 133901 (2003).
[8] M. Padgett and R. Bowman, Nat. Photonics **5**, 343 (2011).
[9] Z. Yan and N. F. Scherer, J. Phys. Chem. Lett. **4**, 2937 (2013).
[10] S. W. Hell and J. Wichmann, Opt. Lett. **19**, 780 (1994).
[11] A. G. Peele, P. J. McMahon, D. Paterson, C. Q. Tran, A. P. Mancuso, K. a. Nugent, J. P. Hayes, E. Harvey, B. Lai, and I. McNulty, Opt. Lett. **27**, 1752 (2002).
[12] T. Brunet, J.-L. Thomas, and R. Marchiano, Phys. Rev. Lett. **105**, 034301 (2010).

[13] J. W. Fleischer, G. Bartal, O. Cohen, O. Manela, M. Segev, J. Hudock, and D. N. Christodoulides, Phys. Rev. Lett. **92**, 123904 (2004).

[14] D. N. Neshev, T. J. Alexander, E. A. Ostrovskaya, Y. S. Kivshar, H. Martin, I. Makasyuk, and Z. Chen, Phys. Rev. Lett. **92**, 123903 (2004).

[15] I. Söllner, S. Mahmoodian, S. L. Hansen, L. Midolo, A. Javadi, G. Kirsanske, T. Pregnolato, H. El-Ella, E. H. Lee, J. D. Song, S. r. Stobbe, and P. Lodahl, Nat. Nanotechnol. **10**, 775 (2015).

[16] A. B. Young, A. C. T. Thijssen, D. M. Beggs, P. Androvitsaneas, L. Kuipers, J. G. Rarity, S. Hughes, and R. Oulton, Phys. Rev. Lett. **115**, 153901 (2015).

[17] Y. Gorodetski, A. Niv, V. Kleiner, and E. Hasman, Phys. Rev. Lett. **101**, 043903 (2008).

[18] N. Shitrit, S. Nechayev, V. Kleiner, and E. Hasman, Nano Lett. **12**, 1620 (2012).

[19] H. Kim, J. Park, S.-W. Cho, S.-Y. Lee, M. Kang, and B. Lee, Nano Lett. **10**, 529 (2010).

[20] A. David, B. Gjonaj, Y. Blau, S. Dolev, and G. Bartal, Optica **2**, 1045 (2015).

[21] N. Ocelic, A. Huber, and R. Hillenbrand, Appl. Phys. Lett. **89**, 101124 (2006).

[22] R. F. Oulton, V. J. Sorger, D. a. Genov, D. F. P. Pile, and X. Zhang, Nat. Photonics **2**, 496 (2008).

[23] M. V. Berry, J. Opt. **15**, 044006 (2013).

[24] E. T. Rogers, J. Lindberg, T. Roy, J. E. Savo, Salvatore anChad, M. R. Dennis, and N. I. Zheludev, Nat. Mater. **11**, 432 (2012).

[25] E. Greenfield, R. Schley, I. Hurwitz, J. Nemirovsky, K. G. Makris, and M. Segev, Opt. Express **21**, 13425 (2013).